Structure and magnetic properties of $Ba_9V_3Te_{15}$ with ferromagnetic spin chains

Jun Zhang[1,2,*] Xinyu Zhang,[3,4,*] Yuanhua Xia,[5,*] Jianfa Zhao,[1,2] Lei Duan[1] Guodong Wang,[1]
Baosen Min,[1] Huibo Cao[6] Clarina R. Dela Cruz,[6] Kan Zhao,[7] Hongyi Sun,[8] Jinlong Zhu,[3,†]
Jianfeng Zhang,[1,2,‡] Tao Xiang,[1,2] Xiancheng Wang[1,2,§] and Changqing Jin[1,2,9,‖]

[1]*Beijing National Laboratory for Condensed Matter Physics, Institute of Physics, Chinese Academy of Sciences, Beijing 100190, China*
[2]*School of Physics, University of Chinese Academy of Sciences, Beijing 100190, China*
[3]*Department of Physics, Southern University of Science and Technology, Shenzhen 518055, China*
[4]*Academy for Advanced Interdisciplinary Studies, Southern University of Science and Technology, Shenzhen 518055, China*
[5]*Key Laboratory of Neutron Physics and Institute of Nuclear Physics and Chemistry, China Academy of Engineering Physics, 621999, Mianyang, China*
[6]*Neutron Scattering Division, Neutron Scattering Science Directorate, Oak Ridge National Laboratory, Oak Ridge, Tennessee 37831, USA*
[7]*School of Physics, Beihang University, Beijing 100191, China*
[8]*Shenzhen Institute for Quantum Science and Engineering, Southern University of Science and Technology, Shenzhen 518055, China*
[9]*Songshan Lake Materials Laboratory, Dongguan, Guangdong 523808, China*

Here we report a ferromagnetic compound $Ba_9V_3Te_{15}$ with quasi-one-dimensional (1D) spin chains. It was synthesized at high-temperature and high-pressure conditions and systematically investigated via structural, transport, magnetic and heat capacity measurements. $Ba_9V_3Te_{15}$ mainly consists of trimerized face-sharing VTe_6 octahedral chains running along the c axis, which are separated by a distance of 10.184(8) Å, thus demonstrating a strong 1D structural character. $Ba_9V_3Te_{15}$ is a semiconductor with a band gap $\sim$128 meV and undergoes a ferromagnetic transition with $T_C \sim 3.6$ K. Far above T_C, the short-range spin orders due to the intrachain spin coupling have developed, which leads to a negative magnetoresistance effect, the deviation of magnetic susceptibility from the Curie-Weiss law and $T^{1/2}$ dependence of magnetic heat capacity. Our results reveal that $Ba_9V_3Te_{15}$ provides a good opportunity to study the intrinsic properties of a system with quasi-1D ferromagnetic spin chains.

I. INTRODUCTION

One-dimensional (1D) systems usually exhibit exotic physical phenomena that can be dramatically different from those in higher dimensional ones [1]. The spin chain compound of $BaVS_3$ has been extensively studied [2–5], where the face-sharing VS_6 octahedral chains are separated by $\sim$6.75 Å. The stoichiometric $BaVS_3$ shows a metal-insulator transition (MIT) at $\sim$69 K, which corresponds to a Peierls transition arising from its 1D electric subband [3]. Subsequently, it undergoes an incommensurate antiferromagnetic (AFM) transition at 31 K [6]. Between the long-range spin order (LRSO) and MIT transitions, the AFM short-range correlation has formed and developed when temperature decreases. For $BaVS_3$, the AFM transition at 31 K is not accompanied by a considerable entropy change due to the pre-existing short-range spin orders (SRSOs) [7], and the ordered moment of 0.5 μ_B/V estimated from neutron diffraction and NMR for $BaVS_3$ is significantly small relative to the full ordered moment of V^{4+} with $S = 1/2(1\,\mu_B)$ [8].

Hf_5Sn_3Cu-anti-type A_3BX_5 is another well-known system with quasi-1D spin chains [9–20], where the spin chains are separated by a large distance more than 9 Å. For the Ba_3TX_5 compounds, where T denotes 3d transition metal and X is chalcogen element, they usually exhibit semiconducting behavior, and the interchain spin coupling is very small, leading to a very low LRSO transition temperature [10,16,19]. $Ba_9Fe_3Se_{15}$ was reported to consist of trimerized face-sharing $FeSe_6$ octahedral chains, and undergo an incommensurate helical spin order transition at 14 K [16,20]. Spin induced ferroelecticity has been found in the quasi-1D $Ba_9Fe_3Se_{15}$ and the electric polarization dynamics are dramatically different from that of high dimensional ferroelectric system [20]. $Ba_6Cr_2S_{10}$ was reported as a ferrotoroidic candidate material. It is composed of dimerized face-sharing CrS_6 octahedral chains and the spins are antiparallelly aligned along the chain below 10 K, which agrees with 1D ferrotoroidic model of dimerized antiferromagnetic spin chain [19].

$Ba_9V_3Se_{15}$ was reported to consist of trimerized face-sharing VSe_6 octahedral chains running along c axis [10]. Compared with the spin chain distance of $\sim$6.7−7.0 Å in $BaV(S/Se)_3$, the spin chains in $Ba_9V_3Se_{15}$ are separated by a larger distance of $\sim$9.5 Å. As a result, $Ba_9V_3Se_{15}$ exhibits a semiconducting behavior with a band gap of 0.2 eV and undergoes a LRSO transition with $T_N \sim 2.5$ K. The magnetic

---

*Theses authors contributed equally to this work.
†Corresponding author: zhujl@sustech.edu.cn
‡Corresponding author: zjf@iphy.ac.cn
§Corresponding author: wangxiancheng@iphy.ac.cn
‖Corresponding author: jin@iphy.ac.cn

heat capacity is found to be $T^{1/2}$ dependent above T_N, which arises from the spin wave excitation within the decoupled ferromagnetic like spin chains. In addition, following the discovery of $Ba_9V_3Se_{15}$, the sister compound of $Ba_9V_3S_{15}$ has been reported by Almoussawi *et al.*. It is a pity that the transport and magnetic properties have not been experimentally studied because the pure polycrystalline $Ba_9V_3S_{15}$ is challenging to obtain [21].

In this work, we report the discovery of the third compound $Ba_9V_3Te_{15}$ in the $Ba_9V_3X_{15}$ family through substituting Se by Te. Comprehensive structural and physical properties associated with its 1D nature were systematically investigated. $Ba_9V_3Te_{15}$ consists of face-sharing VTe_6 octahedral chains. Its trimerized structure and semiconducting behavior originate in the typical 1D electric band structure of Ba_3VTe_5 with primary structure and uniform chains. The neutron diffraction experiments prove the FM ground state with spins oriented in the *c* axis. A behavior of $T^{1/2}$ dependence of magnetic heat capacity is observed above the LRSO $T_c \sim 3.6$ K, demonstrating 1D FM spin chain property. The susceptibility deviating from Curie-Weiss law and the negative magnetoresistance also imply the formation of the SRSO at 200 K.

II. EXPERIMENTAL AND CALCULATION METHOD

$Ba_9V_3Te_{15}$ polycrystalline was synthesized at high pressure and high temperature conditions. The commercially available crystalline powders of V (Alfa, >99.5% pure), Te (Alfa, >99.999% pure) and lumps of Ba (Alfa, immersed in oil, >99.2% pure) were used as the starting materials. The precursor BaTe was prepared by heating the mixture of Ba blocks and Te powder in an alumina crucible sealed in an evacuated quartz tube at 600 °C for 20 h. Then, the mixture of stoichiometric BaTe, V, and Te were homogenously ground according to a molar ratio 3:1:2 and pressed into a pellet with a diameter of 6 mm. The prepressed pellet was placed in a *h*-BN capsule, which was then put into a graphite tube. High pressure experiments were performed in a 6×600 T cubic high pressure apparatus. After pressure was slowly raised to 6 GPa, the sample was heated to 1200 °C within 4 min and kept for 40 min. After the high pressure and high temperature synthesis process, the black pure polycrystalline sample was obtained.

The powder x-ray diffraction (XRD) was performed on a RigakuUltima VI (3KW) diffractometer using Cu Kα radiation generated at 40 kV and 40 mA. The data was collected at a scanning rate of 1° per min with a scanning step length of 0.02 degree. The Rietveld refinement on the diffraction spectra was conducted with GSAS and EXPGUI packages [22]. The neutron powder diffraction (NPD) experiments were performed at the High Flux Isotope Reactor at the Oak Ridge National Laboratory with neutron wavelength (λ) of 2.4103 Å on HB-3 Triple-axis spectrometer. The magnetic structure was solved using neutron diffraction technique by the FULLPROF Suite [23]. The *dc* magnetic susceptibility was measured using a superconducting quantum interference device. The electronic transport and heat capacity were measured using a physical property measurement system.

The fully spin-polarized electronic structure calculations were carried out with the projector augmented wave method [24,25] as implemented in the VASP package [26–29]. The generalized gradient approximation (GGA) of Perdew-Burke-Ernzerhof type [30] was chosen for the exchange-correlation functional. The kinetic energy cutoff of the plane-wave basis was set to be 350 eV. A 16*16*8 $\boldsymbol{k}$-point mesh was used for the Brillouin zone sampling. The Gaussian smearing method with a width of 0.05 meV was employed for the Fermi surface broadening. In structural optimization, we adopted the experimental measured lattice constants and only relaxed the internal atomic positions until the forces on all atoms were smaller than 0.01 eV/Å. The electronic correlation effect among V 3*d* electrons was incorporated by using the GGA+U formalism of Dudarev *et al.* [31]. The effective Hubbard *U* is set as 3 eV. The spin interaction *J* was calculated by the energy differences between the FM ground state and the AFM (FIM) spin configures as introduced in Ref. [10].

III. RESULTS

A. Structure characterization

The powder XRD pattern for $Ba_9V_3Te_{15}$ is presented in Fig. 1(a). The structural model of $Ba_9V_3Se_{15}$ [10] with space group of *P*-6*c*2 (188) was adopted to carry out the refinement for the XRD data. As seen in Fig. 1(a), the Rietveld refinement is smoothly converged to $\chi^2 = 1.96(7)$, $Rp = 4.0(9)\%$ and $Rwp = 2.8(2)\%$, which leads to the lattice constants $a = 10.184(8)$ Å, $c = 19.948(7)$ Å. The detailed crystallographic data are summarized in Table I. Figure 1(b) shows the NPD patterns for $Ba_9V_3Te_{15}$ collected at 10 K and 0.3 K with an enlarged view to show the magnetic Bragg peaks. Figure 1(c) displays the crystal structure of $Ba_9V_3Te_{15}$ with the projection along the *c* axis. The structure consists of face-sharing VTe_6 octahedral chains running along the *c* axis; the chains are arranged in a triangular lattice in the *ab* plane and separated by a large distance ($\sim$10.18 Å), demonstrating a strong 1D structural characteristic. There are two Wyckoff positions for V atoms: V(1) (0,0,0) and V(2) (0,0,0.1621), leading to a trimerized structure feature with two different intrachain V-V distance values of 3.2333 Å and 3.5077 Å, as shown in Fig. 1(d). Each V ion is surrounded by six Te ions to form face-sharing VTe_6 octahedron chains. The VTe_6 octahedrons are distorted, leading to three different V-Te bond lengths of 2.9387, 2.8606, and 2.8621 Å. Using the bond lengths, according to the bond valence sum $= \sum \exp((r_o - r)/b)$, where the constant $b = 0.37$, $r_o = 2.57$ are used for V-Te octahedron and *r* is the interatomic distance between central ion and coordinated ions, the bond valence sums of V site amounts to be $\sim$2.2 for V(1) and $\sim$2.7 for V(2), which suggests the valence states of V(1) and V(2) are +2 and +3, respectively.

Besides the VTe_6 chains, there are two 1D tellurium chains located in the center of triangular lattice, which are composed of Te(3)-Te(4) ions and Te(5)-Te(6) ions [Figs. 1(c) and 1(d)], respectively. It is noted that the occupation of Te(6) is 0.5. In the Te chains the Te ions are inhomogeneously aligned with Te-Te distance ranging from 2.915(1) Å to 3.434(1) Å. The Te-Te distance of 2.915(1) Å is comparable with that in the $(Te_2)^{2-}$ dimer of Ba_2SnTe_5(2.80 Å)
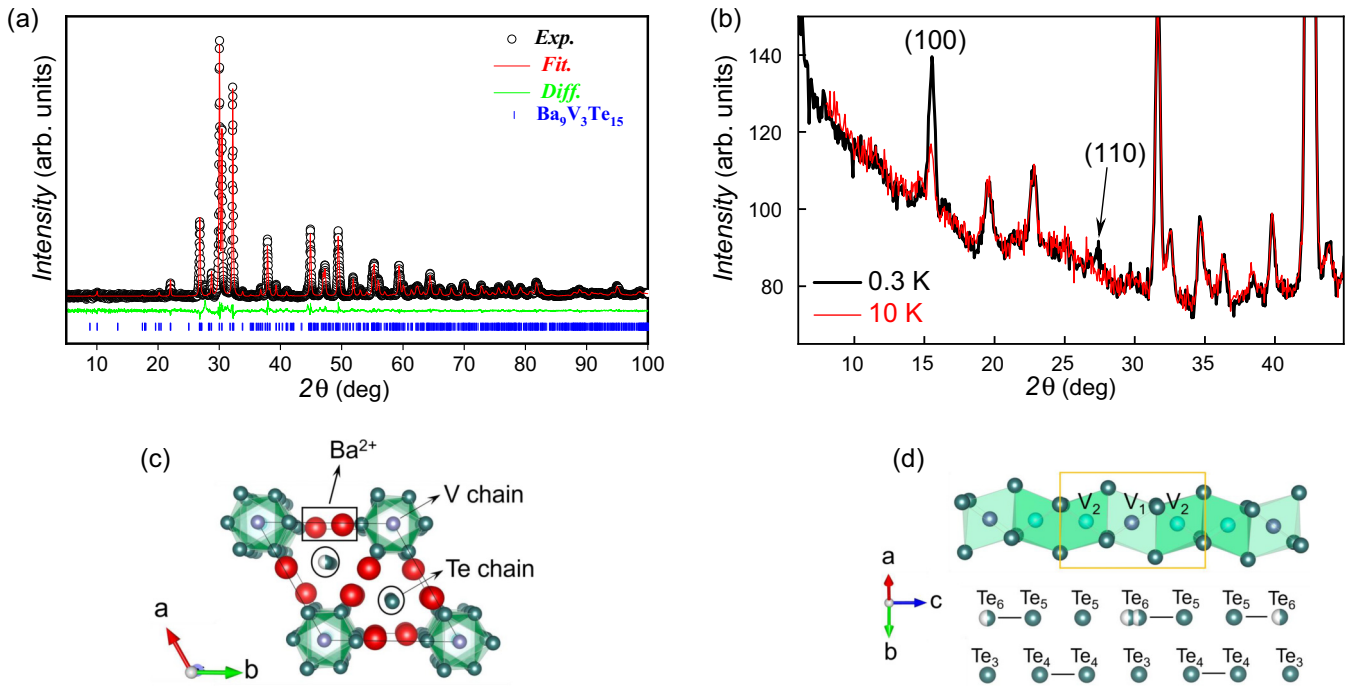
FIG. 1. (a) Powder x-ray diffraction pattern of $Ba_9V_3Te_{15}$ measured at room temperature and ambient pressure and its refinement spectrum. (b) NPD patterns of $Ba_9V_3Te_{15}$. Black and red lines indicate the data collected at 0.3 and 10 K, respectively. (c) The scheme of crystal structure for $Ba_9V_3Te_{15}$, viewing along the axis of the c direction. (d) The trimerized face-sharing VTe_6 octahedral chain and the two Te chains in the center of triangular lattice.

TABLE I. Crystal structure parameters of $Ba_9V_3Te_{15}$.

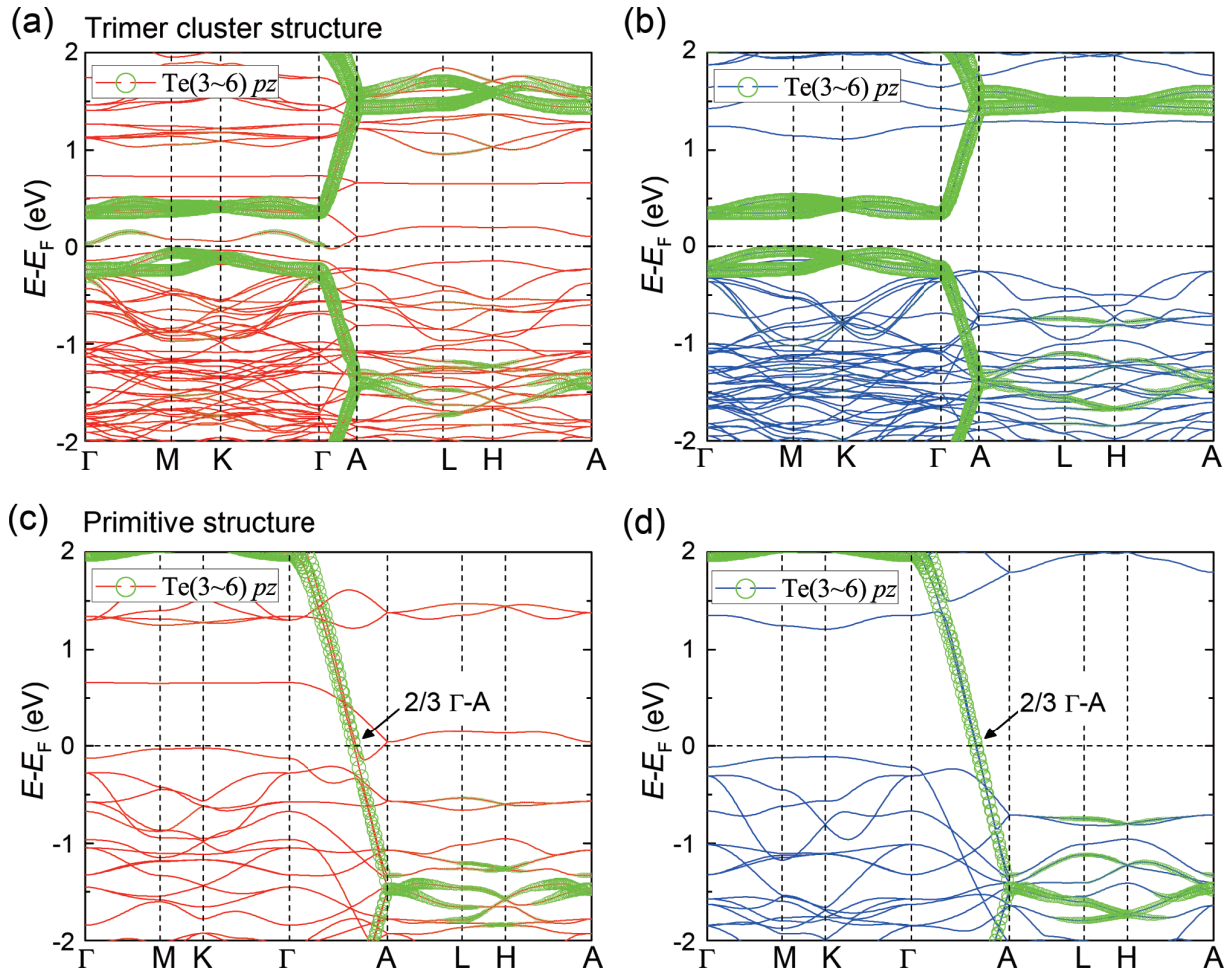| Crystallographic data						
Formula: $Ba_9V_3Te_{15}$				Calculated unit cell formula weight:		
Crystal system: hexagonal				3302.796(0) g/mol		
Space group: P-$6c2$ (188)				Density: 6.12(1) g/cm^3		
Crystal parameters: a = 10.184(8) (Å)				Refined results: χ^2 = 1.96(7)		
c = 19.948(7) (Å) V = 1789.145(0) (Å^3) Z = 2				Rp = 4.0(9)% Rwp = 2.8(2)%		
Atomic parameters						
Atom	wyck.	x	y	z	Uiso	Occ.
Ba_1	12l	0.0121(4)	0.3838(1)	0.0852(6)	0.029(3)	1
Ba_2	6k	0.3813(8)	0.3769(1)	0.25	0.005(5)	1
V_1	2a	0	0	0	0.016(5)	1
V_2	4g	0	0	0.1621(5)	0.014(1)	1
Te_1	12l	0.2380(1)	0.2345(9)	0.0845(1)	0.023(3)	1
Te_2	6k	0.0091(6)	0.2264(3)	0.25	0.003(1)	1
Te_3	2c	1/3	2/3	0	0.046(6)	1
Te_4	4h	1/3	2/3	0.1694(3)	0.039(1)	1
Te_5	4i	2/3	1/3	0.1638(5)	0.014(8)	1
Te_6	4i	2/3	1/3	0.0177(6)	0.022(2)	0.5
Bond length (Å)						
V_1 − Te_1	V_2−Te_2	V_2−Te_1	Te_3−Te_4	Te_4 − Te_4	Te_5−Te_5	Te_5−Te_6
2.938(7)	2.862(1)	2.860(6)	3.379(7)	3.215(1)	3.434(1)	2.915(1)
Bond angle (°)				Distance of the adjacent V atoms (Å)		
Te_1−V_1−Te_1		Te_1−V_2−Te_2		V_1−V_2		V_2−V_2
178.8(2)		174.8(6)		3.233(3)		3.507(7)

FIG. 2. (a) and (b) The calculated band structures of different spin channels for the ferromagnetic $Ba_9V_3Te_{15}$ with trimer cluster distortion. The red lines represent the spin up channel while the blue lines for the spin-down channel. The green circles on the band structure represent the weight of Te(3 ∼ 6) atomic **pz** orbitals. (c) and (d) similar with (a) and (b) but adopting the primitive structure without any CDW distortion.

[32] and in $Ba_9Sn_3Te_{15}$(2.78 Å) [9]. It implies that partial covalent bonds exist in the Te chains, which has also been observed in its sister compounds of $Ba_9V_3Se_{15}$ [10] and $Ba_9V_3S_{15}$ [21]. Based on the site symmetry and the charge balance, the molecular formula of $Ba_9V_3Te_{15}$ can be rewritten as $Ba_9V_3(Te^{2-})_9(Te_2^{2-}Te_4^{1-})$. For comparison, the degree of trimerization is defined by the ratio of $|d_{inter} - d_{intra}|/|d_{inter} + d_{intra}|$, where d_{inter} is the distance of the adjacent V(2) atoms and d_{intra} is that of the adjacent V(1) and V(2) atoms. The calculated value of 0.0407 for $Ba_9V_3Te_{15}$ is obviously smaller than that of 0.0549 for the $Ba_9V_3Se_{15}$. The weaker electronegativity of Te should be responsible for the smaller structure distortion as will be discussed in the following.

For clarifying the origin of the inhomogeneous VTe_6 and Te(3 ∼ 6) chain in $Ba_9V_3Te_{15}$, we performed the electron structure calculation for both the trimerized case of $Ba_9V_3Te_{15}$ and the primary structure of Ba_3VTe_5 with uniform VT_6 chain similar to the structure of Ba_3TiTe_5 [11]. Comparing with the distorted case in Figs. 2(a) and 2(b), the calculations for a uniform chain of Ba_3VTe_5 present a new continuous Te(3 ∼ 6) atomic **pz** orbitals dominated quasi-1D

band structure cross the Fermi level (green circles on band structure) as shown in Figs. 2(c) and 2(d). The corresponding Fermi surfaces are nearly the $kz = \pm 1/3c_0^*(\pm 2/3\Gamma - A$ point) plane. These quasi-1D Fermi surfaces form an obvious nesting by a vector of $q = \pm 1/3c_0^*$. This prominent nesting vector should further induce a charge density wave (CDW)-like lattice instability with a CDW vector of $q_{CDW} = 1/3\,c_0^*$. The CDW supercell at least includes three Te atoms along Te(3 ∼ 6) atom chain, as shown in the Fig. 1(d). Within the trimer distortion structure, the quasi-1D band from Te **pz** orbital is gapped and keeps far away from the Fermi level as shown in Figs. 2(a) and 2(b). Considering the great CDW gap (0.56 eV) and atomic distortion degree (Te-Te bond lengths from 2.91 Å to 3.43 Å), the CDW transition temperature (T_{CDW}) should be far higher than other typical CDW materials [33,34]. Through our studied temperature region, the system is always in its distorted CDW phase. Besides the direct influence on the Te(3 ∼ 6) atomic 1D electron structure, the trimer cluster distortion of Te chains can also induce the trimer cluster distortion of V chains and band renormalization of the magnetic V atoms in the 1D VTe_6 octahedral chain with same trimer supercell.
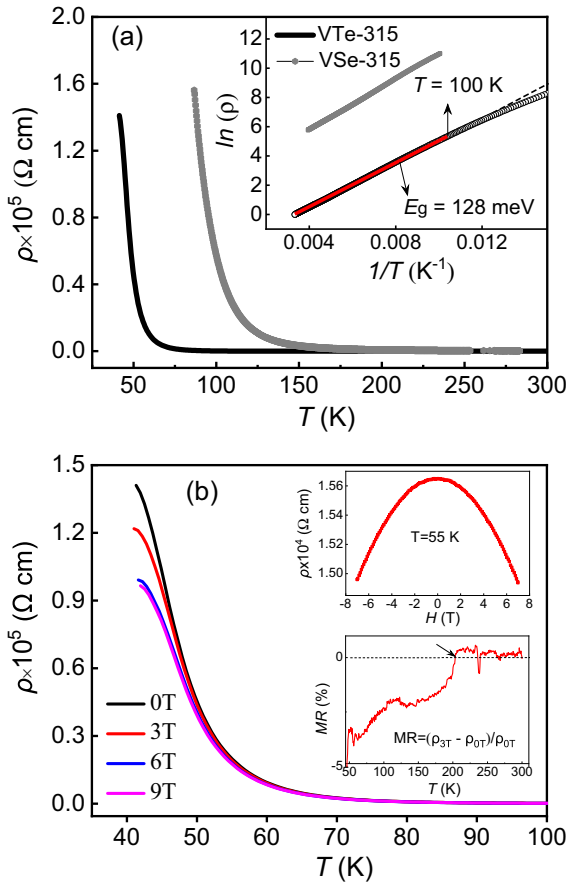
FIG. 3. (a) The temperature dependence of resistivity for $Ba_9V_3Te_{15}$ and $Ba_9V_3Se_{15}$, respectively. The inset shows the $\ln(\rho)$ versus inverse temperature $(1/T)$ and the linear fit. (b) The Resistivity measured under magnetic fields with H up to 9 T for $Ba_9V_3Te_{15}$. The upper inset is ρ vs H measured at 55 K, and the lower inset is the temperature dependence of MR.

B. Transport and magnetic properties

Figure 3(a) displays the temperature dependence of electrical resistivity (ρ) for $Ba_9V_3Te_{15}$. The resistivity is approximate 0.99(3) Ω cm at room temperature and increases with the decrease of temperature (i.e., $d\rho/dT < 0$), demonstrating a typical semiconductor characteristic. The inset shows the curve of $\ln(\rho)$ versus $1/T$. It presents a straight line between 100 and 300 K, which indicates that the intrinsic electrical conductivity is dominated by thermal activation mechanism. By using the formula of $\rho \propto \exp(\Delta_g/2k_BT)$, where Δ_g is the semiconducting band gap and k_B is the Boltzmann constant, the resistivity curve can be well fitted and the band gap Δ_g is estimated to be 0.128 eV. Figure 3(b) shows the resistivity curves measured under different magnetic field. It is seen that the resistivity decreases when magnetic field is applied at low temperature range, demonstrating a negative magnetoresistance (MR) effect. The negative MR also can be clearly seen as the field dependence of resistance measured at 55 K shown in the upper inset of Fig. 3(b). The lower inset of Fig. 3(b) displays the resistivity difference between 0 and 3 T. The negative MR $= (\rho_{(3T)} - \rho_{(0T)})/\rho_{(0T)}$ develops

from $\sim$200 K. Generally, the negative MR is related to FM correlation and will be discussed latter.

The magnetic properties of $Ba_9V_3Te_{15}$ were studied via the magnetic susceptibility and neutron diffraction measurements. Fig. 4(a) presents the temperature dependence of susceptibility measured under the field of 100 Oe. The magnetic susceptibility increases sharply at $\sim$4 K, demonstrating a typical FM-like phase transition. The magnetization curves measured under different external magnetic field H are presented in Fig. 4(b) and the temperature derivative of magnetization are shown in the inset. From the peak of $d\chi/dT$ of H = 100 Oe, the LRSO transition temperature can be determined to be 3.6 K. The peak gradually shifts towards high temperature as H increasing, which is a general property for a FM system. The isothermal magnetization measured at different temperature are displayed in Fig. 4(c). The magnetization exhibits linear magnetic field dependent behavior above 4 K, while it is featured with a S-shape below 4 K; this further confirms the formation of LRSO at the temperature close to 4 K. The magnetized moment is about 4.2 $\mu_B/f.u.$ at $H = 7$ T and 1.8 K, as shown in the inset of Fig. 4(c).

The inverse susceptibility for $H = 100$ Oe is also shown in Fig. 4(a), where the linear temperature dependence of $1/\chi$ is only observed in high temperature range. According to the Curie-Weiss law $1/\chi = (T - T_\theta)/C$, the linear fitting between 200 and 300 K gives the effective moment $\mu_{eff} = 5.87$ $\mu_B/f.u.$ and Weiss temperature $T_\theta = 48$ K, respectively. As suggested by the structural analysis, the valence state of V(1) is +2 with S = 3/2 and V(2) is +3 with S = 2/2. The theoretical value of the effective moment of $Ba_9V_3Te_{15}$ can also be estimated to be $g\mu_B\sqrt{\frac{3}{2} \times (\frac{3}{2} + 1) + 2 \times \frac{2}{2} \times (\frac{2}{2} + 1)} = 5.6$ μ_B with the Landé factor $g = 2$. Therefore, the effective moment from valance state analysis is consistent with the magnetic susceptibility experiment. The positive T_θ value suggests the dominated spin coupling is ferromagnetic in $Ba_9V_3Te_{15}$. The electronic configuration state of V on average is $3d^{7/3}$ in $Ba_9V_3Te_{15}$, thus the saturation moment should be 7 $\mu_B/f.u.$ if all spins are ferromagnetic aligned; this value is much higher than the magnetized moment value of $\sim$4.2 $\mu_B/f.u.$ measured at 7 T and 1.8 K. This is a common phenomenon for the quasi-1D spin chain system due to the quantum or thermal fluctuation. Such a reduced magnetized moment has also been reported in $Ba_6Cr_2S_{10}$ and $KCuF_3$ with weakly coupled spin chains [19,35]. For $KCuF_3$ a saturated moment of 0.5 μ_B/Cu^{2+} was reported with a 50% reduction relative to the fully ordered moment for Cu^{2+} (S = 1/2) [35].

In order to clarify the magnetic structure of $Ba_9V_3Te_{15}$, the NPD measurements were performed. Figure 1(b) shows NPD patterns for $Ba_9V_3Te_{15}$ collected at 10 and 0.3 K. Clear differences between the two diffraction patterns are the enhancement of peaks at $2\theta = 15$ and 27.4 degree, indexed as (100) and (110), respectively. It is originated from the magnetic lattice of $Ba_9V_3Te_{15}$ with respect to that collected at 10 K. The lack of a magnetic contribution to the (001) reflection implies that the magnetic moments point along the c axis. By the Rietveld refinement for the NPD pattern of $Ba_9V_3Te_{15}$ collected at 0.3 K, as seen in the Supplemental Material [36], the magnetic moment of V(1) at $2a$ site is estimated to be 1.616 μ_B and V(2) at $4g$ site 0.333 μ_B. The ordered moment provided by neutron diffraction in $Ba_9V_3Te_{15}$ is
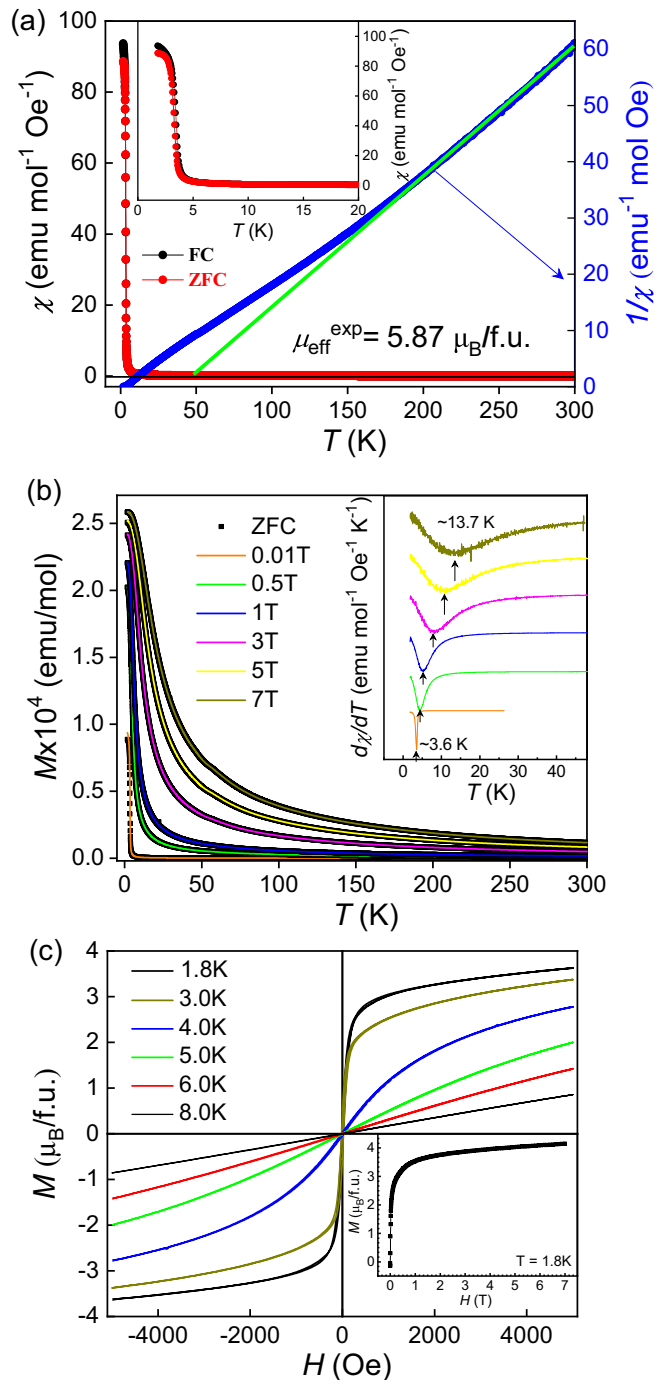
FIG. 4. The magnetic properties of $Ba_9V_3Te_{15}$. (a) Temperature dependence of susceptibility $\chi(T)$ and inverse susceptibility $\chi^{-1}(T)$ measured in zero-field-cooled (ZFC) and field-cooled (FC) modes under $H = 100$ Oe. The green line is the linear fitting within temperature range of 200–300 K. (b) The temperature dependence of magnetization collected at different H. The inset shows the $d\chi/dT(T)$ curves to determine T_C. (c) The isothermal magnetization collected at different temperature. The inset shows magnetization measurement at 1.8 K with a magnetic field up to 7 T.

about 2.3 μ_B/f.u., which is 1.9 μ_B/f.u. smaller than the magnetized moment measured at 7 T and 1.8 K. It is suggested that strong quantum or thermal fluctuation exists in the system. Applying a magnetic field can overcome the spin fluctuation
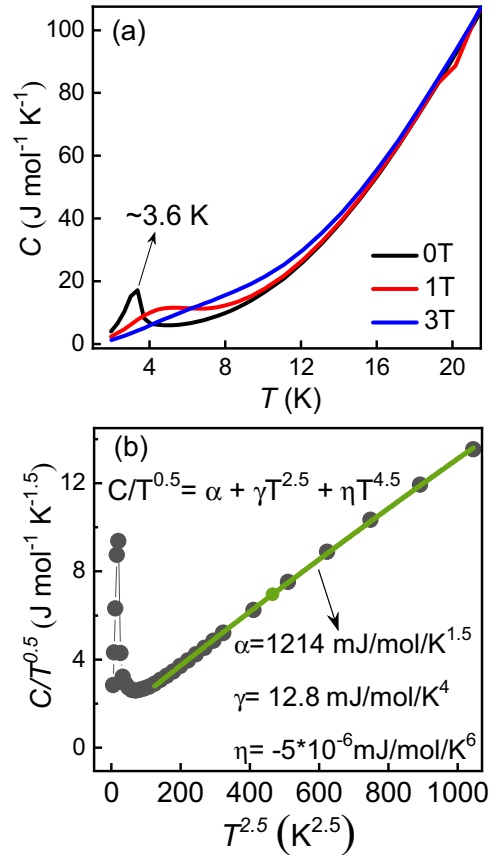

FIG. 5. (a) Temperature dependence of heat capacity $C(T)$ for $Ba_9V_3Te_{15}$ measured under 0–3 T external field. (b) The heat capacity data is plotted as $C/T^{1/2}$ versus $T^{5/2}$. The dark green line is the fit using the equation of $C/T^{0.5} = \alpha + \beta T^{2.5} + \eta T^{4.5}$.

and further orientate the fluctuated spins, leading to an enhancement of the magnetized moment. In addition, it is known that SRSOs usually contribute to the magnetic diffuse scattering and lead to a higher background. However, as discussed below, there exist SRSOs in individual spin chains in both cases of above and below the LRSO temperature. This is why we just observe little difference between the background of the spectrums collected at 10 and 0.3 K.

C. Heat capacity measurements

Figure 5(a) displays the temperature dependence of heat capacity (HC) $C(T)$ data measured under different magnetic fields. For the $C(T)$ data with $H = 0$ T there is a small peak centered at ~3.6 K, corresponding to the LRSO transition. With applying field increasing, the heat capacity peak shifts to higher temperature region and becomes broader, which is consistent with a general FM characteristic. Just above the LRSO transition, the chains are completely decoupled and the spin wave excitation arising from the spin chains should have significant contributions to the HC. As predicted by the spin wave theory, ferromagnetic chains host a quadratic magnon excitation with $\omega \sim k^2$, which should lead to a $T^{1/2}$ magnetic HC at low temperature. Since $Ba_9V_3Te_{15}$ is a semiconductor, the contribution of HC from itinerant electrons can be ignored. Thus, we can estimate the coefficient of the magnetic

contribution of $\alpha T^{1/2}$ via the $C(T)$ data divided by $T^{1/2}$ as plotted in Fig. 5(b). By fitting the data using the equation of $C/T^{1/2} = \alpha + \beta T^{5/2} + \eta T^{9/2}$, the coefficient α can be obtained to be 1.214 J/mol/K$^{1.5}$, which of the value is related to the intrachain coupling strength.

IV. DISCUSSION

Ba$_9$V$_3$Te$_{15}$ exhibits strong 1D magnetic properties. For an ideal spin chain, LRSO cannot form at finite temperature because of strong quantum or thermal fluctuation due to the dimension reduction. While for a quasi-1D spin chain system, the interchain spin coupling strength J_{inter} is typically two or three orders of magnitude lower than that of intrachain coupling J_{intra}. However, J_{inter} governs the LRSO formation, although it is very weak [37]. Far above the LRSO temperature, the spin chains are completely decoupled and SRSOs have already formed due to the large J_{intra} and developed when temperature decreases. It is supposed that below LRSO temperature only partial SRSOs with long correlation length are coupled by J_{inter} to form LRSO. The remainder of the SRSOs with short correlation length should still be decoupled and randomly exist in individual spin chains, and this might be the reason that a reduced magnetized moment is usually observed in quasi-1D spin chain system. For Ba$_9$V$_3$Te$_{15}$, the magnetized moment measured at 7 T and 1.8 K is about 4.2 μ_B/f.u., which is much smaller than the expected value of 7 μ_B/f.u. for a fully ordered state. In addition, above $H = 2.5$ T the magnetized moment increases linearly with H, implying that applying high H can partially overcome the spin fluctuation and orientate the SRSOs to further enhance the magnetized moment. The reduced magnetized moment and nonsaturated moment suggest strong spin fluctuation in Ba$_9$V$_3$Te$_{15}$, which is one of the 1D magnetic characters.

The formation of SRSOs due to the intrachain spin coupling far above the LRSO is another typical character for the 1D magnetic system. The magnetic contribution to HC associated with 1D spin wave excitation above LRSO directly demonstrates the existence of SRSOs in Ba$_9$V$_3$Te$_{15}$. In addition, the susceptibility obviously deviates from the Curie-Weiss behavior below ~200 K, also implying SRSOs have formed far above the LRSO temperature. At high temperature the spin chains are decoupled and SRSOs have already gradually developed as temperature decreases before LRSO formation. The gradual development of SRSOs should cause a variation of the Weiss constant depending on temperature and lead to the deviation from Curie-Weiss law. The formation of SRSOs also can be demonstrated by the negative magnetoresistance phenomenon. Since the intrachain coupling is ferromagnetic, the formation of ferromagnetic SRSOs would lead to a negative MR behavior because magnetic field can orientate the SRSOs and reduce the electron scattering. The negative MR occurs at 200 K, consistent with that where the susceptibility begins to deviate from Curie-Weiss behavior. Therefore, it is suggested that the deviation of susceptibility from Curie-Weiss behavior and negative MR should have the same origin, i.e., the formation of SRSOs.

Besides, dimensionality has profound effects on CDW instabilities [38]. Especially, the Fermi surface nesting in the reduced dimensional system can induce a CDW-like lattice instability, favoring the formation of CDW supercell. In the previous work [19], the quasi-1D chain compound with the dimer structure was reported, which can be well understood as that the reduced dimensionality strengthens the Peierls instabilities due to the Fermi surface nesting, and induces the CDW instabilities and dimerized structure distortion. In the present work, the trimerized structure in Ba$_9$V$_3$Te$_{15}$ is mainly caused by the Fermi surface nesting originated from the in-chain Te atomic pz bands. In the Ba$_9$V$_3$X$_{15}$ (X = S, Se, Te) system, the Te element in Ba$_9$V$_3$Te$_{15}$ has the weakest electronegativity. Therefore, along the 1D Te chain, the weaker covalent bond between the Te atoms makes the Te chains have less distortion than that in Ba$_9$V$_3$Se$_{15}$ and Ba$_9$V$_3$S$_{15}$ and thus, leads to a reduced trimeric cluster distortion for the VTe$_6$ chains, which agrees with the comparison of trimerization degree between Ba$_9$V$_3$Te$_{15}$ and Ba$_9$V$_3$Se$_{15}$.

For Ba$_9$V$_3$Te$_{15}$, our DFT calculations suggests a reduced difference between J_1 (the nearest-neighbor coupling between V$_1$-V$_2$) and J_2 (the next-nearest-neighbor coupling between V$_2$-V$_2$) with a ratio of J_2/J_1 about 0.658, which is far larger than that in Ba$_9$V$_3$Se$_{15}$($J_2/J_1 = 0.006$) [10] and Ba$_9$V$_3$S$_{15}$ ($J_2/J_1 = 0.028$) [21] systems. Considering the small difference between J_1 and J_2, we can coarsely estimate the intrachain spin coupling based on a model of homogeneous ferromagnetic spin chain with an averaged spin value (S = 1/2*7/3) for V ions. The formation of SRSOs is suggested to occur at ~200 K by the magnetic susceptibility and negative MR experiments. By using the equation of $k_B T = \frac{2}{3}zS(S + 1)J_{intra}$, where k_B is the Boltzmann constant, $z = 2$ is the number of nearest-neighbor magnetic atoms for spin chains, $T = 200$ K denotes the SRSOs formation temperature, and the local moment $S = 7/6$, we can calculate the J_{intra} to be 6.5 meV. Also, we can estimate the J_{intra} value from the HC data. For idea ferromagnetic spin chain, the magnetic contribution to the heat capacity can be expressed by the equation:

$$C/R = \frac{3}{4}\frac{\zeta(3/2)}{\sqrt{2\pi}}\left(\frac{k_B}{2SJ}\right)^{0.5}T^{0.5},$$

where R is the idea gas constant, k_B is Boltzmann constant, and the Zeta function of $\zeta(3/2) = 2.61238$ [39]. From the obtained coefficient of $T^{0.5}$ term by the heat capacity experiments ($\alpha = 0.404$ J/mol/K$^{1.5}$ for Ba$_3$VTe$_5$ with uniform spin chain), the J_{intra} value can be determined to be 9.5 meV, which is very close to that obtained from magnetic susceptibility and negative MR experiments.

The discovery of Ba$_9$V$_3$Te$_{15}$ completes the family of Ba$_9$V$_3$X$_{15}$ (X = S, Se and Te). Thus, we have a comparison of the lattice parameters among the three compounds, which is shown in the Supplemental Material [36]. The distance between the adjacent VX$_6$ chains is more than 9 Å for all the three compounds. While X anion varies from S to Te, the crystal lattice constants a and c increase monotonously due to the increase of anion size. The resistivity data of Ba$_9$V$_3$Se$_{15}$, taken from Ref. [10], is also presented in Fig. 3(a). Since pure Ba$_9$V$_3$S$_{15}$ sample is hard to be synthesized, the resistivity data is absent. Obviously, the band gap of Ba$_9$V$_3$Te$_{15}$ is smaller than Ba$_9$V$_3$Se$_{15}$. As shown in Fig. 2, the valence band maximum and conduction band minimum are dominated by

the in-chain Te p_z orbital. Compared with $Ba_9V_3Se_{15}$, the less distortion of Te-chain in $Ba_9V_3Te_{15}$ would open a smaller gap although its crystal lattice is larger.

V. CONCLUSION

A quasi-1D FM semiconductor of $Ba_9V_3Te_{15}$ was synthesized under high-temperature and high-pressure conditions. It crystallizes in a hexagonal structure with the space group P-$6c2$ (No. 188), which consists of 1D VTe_6 chains separated by 10.184(8) Å. $Ba_9V_3Te_{15}$ undergoes a FM LRSO transition at 3.6 K with the spin oriented along the c axis. Above T_C the resistance shows negative MR, the susceptibility deviates from the Curie-Weiss behavior, and a large magnetic heat capacity is observed and proportional to $T^{1/2}$, following the prediction for 1D FM spin chain. All these exotic phenomena demonstrate that SRSOs associated with the intrachain coupling have gradually developed above T_C, which is indicative of the nature of quasi-1D spin chains.

[1] T. Giamarchi, *Quantum Physics in One Dimension, International Series of Monographs on Physics* (Oxford University Press, Oxford, 2003).

[2] S. Fagot, P. Foury-Leylekian, S. Ravy, J. P. Pouget, and H. Berger, One-dimensional instability in $BaVS_3$, Phys. Rev. Lett. **90**, 196401 (2003).

[3] L. Forro, R. Gaal, H. Berger, P. Fazekas, K. Penc, I. Kezsmarki, and G. Mihaly, Pressure induced quantum critical point and non-fermi-liquid behavior in $BaVS_3$, Phys. Rev. Lett. **85**, 1938 (2000).

[4] P. Leininger, V. Ilakovac, Y. Joly, E. Schierle, E. Weschke, O. Bunau, H. Berger, J. P. Pouget, and P. Foury-Leylekian, Ground state of the quasi-1D compound $BaVS_3$ resolved by resonant magnetic x-ray scattering, Phys. Rev. Lett. **106**, 167203 (2011).

[5] F. Lechermann, S. Biermann, and A. Georges, Importance of interorbital charge transfers for the metal-to-insulator transition of $BaVS_3$, Phys. Rev. Lett. **94**, 166402 (2005).

[6] J. Kelber, A. T. Aldred, G. H. Lander, M. H. Mueller, O. Massenet, and G. D. Stucky, Magnetization and neutron study of $BaVS_3$, J. Solid State Chem. **32**, 351 (1980).

[7] G. Mihály, I. Kézsmárki, F. Zámborszky, M. Miljak, K. Penc, P. Fazekas, H. Berger, and L. Forró, Orbitally driven spin pairing in the three-dimensional nonmagnetic Mott insulator $BaVS_3$: Evidence from single-crystal studies, Phys. Rev. B **61**, R7831(R) (2000).

[8] H. Nakamura, T. Yamasaki, S. Giri, H. Imai, M. Shiga, K. Kojima, M. Nishi, K. Kakurai, and N. Metoki, Incommensurate magnetic ordering and spin-liquid-like state in a triangular lattice $BaVS_3$: Neutron diffraction and scattering study, J. Phys. Soc. Jpn. **69**, 2763 (2000).

[9] J. Zhang, R. Su, X. Wang, W. Li, J. Zhao, Z. Deng, S. Zhang, S. Feng, Q. Liu, H. Zhao, P. Guan, and C. Jin, Synthesis, crystal structures, and electronic properties of one dimensional $Ba_9Sn_3(Te_{1-x}Se_x)_{15}$ ($x = 0$–1), Inorg. Chem. Front. **4**, 1337 (2017).

[10] J. Zhang, M. Liu, X. C. Wang, K. Zhao, W. M. Li, L. Duan, J. F. hao, L. P. Cao, G. Y. Dai, Z. Deng, S. J. Zhang, S. M. Feng, Q. Q. Liu, Y. F. Yang, and C. Q. Jin, $Ba_9V_3Se_{15}$: A novel compound with spin chains, J. Phys.: Condens. Matter **30**, 214001 (2018).

[11] J. Zhang, Y. Jia, X. Wang, Z. Li, L. Duan, W. Li, J. Zhao, L. Cao, G. Dai, Z. Deng, S. Zhang, S. Feng, R. Yu, Q. Liu, J. Hu, J. Zhu, and C. Jin, A new quasi-one-dimensional compound Ba_3TiTe_5 and superconductivity induced by pressure, NPG Asia Mater. **11**, 60 (2019).

[12] J. Zhang, L. Duan, Z. Wang, X. C. Wang, J. F. Zhao, M. L. Jin, W. M. Li, C. L. Zhang, L. P. Cao, Z. Deng, Z. W. Hu, S. Agrestini, M. Valvidares, H.-J. Lin, C.-T. Chen, J. L. Zhu, and C. Q. Jin, The synthesis of a quasi-one-dimensional iron-based telluride with antiferromagnetic chains and a spin glass state, Inorg. Chem. **59**, 5377 (2020).

[13] L. Duan, X. C. Wang, J. Zhang, J. F. Zhao, L. P. Cao, W. M. Li, R. Z. Yu, Z. Deng, and C. Q. Jin, Synthesis, structure, and properties of $Ba_9Co_3Se_{15}$ with one-dimensional spin chains, Chin. Phys. B **29**, 036102 (2020).

[14] L. Duan, X. C. Wang, F. Y. Zhan, J. Zhang, Z. W. Hu, J. F. Zhao, W. M. Li, L. P. Cao, Z. Deng, R. Z. Yu, H. J. Lin, C. T. Chen, R. Wang, and C. Q. Jin, High-pressure synthesis, crystal structure and physical properties of a new Cr-based arsenide La_3CrAs_5, Sci. China Mater. **63**, 1750 (2020).

[15] J. Zhang, M. L. Jin, X. Li, X. C. Wang, J. F. Zhao, Y. Liu, L. Duan, W. M. Li, L. P. Cao, B. J. Chen, L. J. Wang, F. Sun, Y. G. Wang, L. X. Yang, Y. M. Xiao, Z. Deng, S. M. Feng, C. Q. Jin, and J. L. Zhu, Structure-spin-transport anomaly in quasi-1-dimensional $Ba_9Fe_3Te_{15}$ under high pressure, Chin. Phys. Lett. **37**, 087106 (2020).

[16] J. Zhang, A. C. Komarek, M. Jin, X. Wang, Y. Jia, J. Zhao, W. Li, Z. Hu, W. Peng, X. Wang, L. H. Tjeng, Z. Deng, R. Yu, S. Feng, S. Zhang, M. Liu, Y.-f. Yang, H.-j. Lin, C.-T. Chen, X. Li, J. Zhu, and C. Jin, High-pressure synthesis, crystal structure,

and properties of iron-based spin-chain compound $Ba_9Fe_3Se_{15}$, Phys. Rev. Mater. **5**, 054606 (2021).

[17] L. Duan, X.-C. Wang, J. Zhang, J.-F. Zhao, W.-M. Li, L.-P. Cao, Z.-W. Zhao, C. Xiao, Y. Ren, S. Wang, J. Zhu, and C.-Q. Jin, Doping effect on the structure and physical properties of quasi-one-dimensional compounds $Ba_9Co_3(Se_{1-x}S_x)_{15}$ (x = 0–0.2), Chin. Phys. B **30**, 106101 (2021).

[18] L. Duan, X. C. Wang, J. Zhang, Z. Hu, J. F. Zhao, Y. G. Feng, H. L. Zhang, H. J. Lin, C. T. Chen, W. Wu, Z. Li, R. Wang, J. F. Zhang, T. Xiang, and C. Q. Jin, Synthesis, structure, and magnetism in the ferromagnet La_3MnAs_5: Well-separated spin chains coupled via itinerant electrons, Phys. Rev. B **106**, 184405 (2022).

[19] J. Zhang, X. C. Wang, L. Zhou, G. X. Liu, D. T. Adroja, I. da Silva, F. Demmel, D. Khalyavin, J. Sannigrahi, H. S. Nair, L. Duan, J. F. Zhao, Z. Deng, R. Z. Yu, X. Shen, R. C. Yu, H. Zhao, J. M. Zhao, Y. W. Long, Z. W. Hu, H. J. Lin, T. S. Chan, C. T. Chen, W. Wu, and C. Q. Jin, A ferrotoroidic candidate with well-separated spin chains, Adv. Mater. **34**, 2106728 (2022).

[20] J. Zhang, X. Wang, Y. Hao, G. Liu, L. Zhou, D. M. Pajerowski, J. Wang, J. Zhu, J. Zhao, J. Wang, Y. Zhao, C. Duan, Y. Long, C.-J. Kang, M. Greenblatt, and C. Jin, Ferroelectricity driven by magnetism in quasi-one-dimensional $Ba_9Fe_3Se_{15}$, arXiv:2207.10834.

[21] B. Almoussawi, H. Tomohiri, H. Kageyama, and H. Kabbour, High pressure synthesis of the spin chain sulfide $Ba_9V_3S_{11}(S_2)_2$, Eur. J. Inorg. Chem. **2021**, 1271 (2021).

[22] A. C. Larson and R. B. Von Dreele, General Structure Analysis System (GSAS), Los Alamos National Laboratory Report LAUR, 2000, p. 86.

[23] J. Rodríguez-Carvajal, Recent advances in magnetic-structure determination by neutron powder diffraction, Physica B **192**, 55 (1993).

[24] P. E. Blochl, Projector augmented-wave method, Phys. Rev. B **50**, 17953 (1994).

[25] G. Kresse and D. Joubert, From ultrasoft pseudopotentials to the projector augmented-wave method, Phys. Rev. B **59**, 1758 (1999).

[26] G. Kresse and J. Hafner, *Ab initio* molecular dynamics for liquid metals, Phys. Rev. B **47**, 558 (1993).

[27] G. Kresse and J. Hafner, Norm-conserving and ultrasoft pseudopotentials for first-row and transition elements, J. Phys.: Condens. Matter **6**, 8245 (1994).

[28] G. Kresse and J. Furthmller, Efficiency of *ab-initio* total energy calculations for metals and semiconductors using a plane-wave basis set, Comp. Mater. Sci **6**, 15 (1996).

[29] G. Kresse, Efficient iterative schemes for *ab initio* total-energy calculations using a plane-wave basis set, Phys. Rev. B **54**, 11169 (1996).

[30] J. P. Perdew, K. Burke, and M. Ernzerhof, Generalized gradient approximation made simple, Phys. Rev. Lett. **77**, 3865 (1996).

[31] S. L. Dudarev, G. A. Botton, S. Y. Savrasov, C. J. Humphreys, and A. P. Sutton, Electron-energy-loss spectra and the structural stability of nickel oxide: An LSDA+U study, Phys. Rev. B **57**, 1505 (1998).

[32] A. Assoud, S. Derakhshan, N. Soheilnia, and H. Kleinke, Electronic structure and physical properties of the semiconducting polytelluride Ba_2SnTe_5 with a unique Te_5^{4-} unit, Chem. Mater. **16**, 4193 (2004).

[33] B. Burk, R. E. Thomson, J. Clarke, and A. Zettl, Surface and bulk charge-density wave structure in $1T$-TaS_2, Science **257**, 362 (1992).

[34] X. Xi, L. Zhao, Z. Wang, H. Berger, L. Forro, J. Shan, and K. F. Mak, Strongly enhanced charge-density-wave order in monolayer $NbSe_2$, Nat. Nanotechnol. **10**, 765 (2015).

[35] B. Lake, D. A. Tennant, C. D. Frost, and S. E. Nagler, Quantum criticality and universal scaling of a quantum antiferromagnet, Nat. Mater. **4**, 329 (2005).

[36] See Supplemental Material at http://link.aps.org/supplemental/10.1103/PhysRevB.108.174423 for the lattice constants evolution as chalcogen ions change from S to Te in $Ba_9V_3X_{15}$ (X = S, Se and Te); NPD spectrum collected at 10 K and 0.3 mK.

[37] M. F. Collins and O. A. Petrenko, Triangular antiferromagnets, Can. J. Phys. **75**, 605 (1997).

[38] M. Calandra, I. I. Mazin, and F. Mauri, Effect of dimensionality on the charge-density wave in few-layer 2H-NbSe_2, Phys. Rev. B **80**, 241108(R) (2009).

[39] M. Takahashi, Quantum Heisenberg ferromagnets in one and two dimensions at low temperature, Prog. Theor. Phys. Suppl. **87**, 233 (1986).